Geosci. Model Dev. Discuss., 8, 6379–6415, 2015
www.geosci-model-dev-discuss.net/8/6379/2015/
doi:10.5194/gmdd-8-6379-2015

Geoscientific Model Development Discussions
Open Access

DebrisInterMixing-2.3: a Finite Volume solver for three dimensional debris flow simulations based on a single calibration parameter – Part 2: Model validation

A. von Boetticher[1,3], J. M. Turowski[2,3], B. W. McArdell[3], D. Rickenmann[3], M. Hürlimann[4], C. Scheidl[5], and J. W. Kirchner[1,3]

[1]Department of Environmental Systems Science, Swiss Federal Institute of Technology Zurich ETHZ, CHN H41 8092 Zürich, Switzerland
[2]Helmholtz-Centre Potsdam GFZ German Research Center for Geosciences, Telegrafenberg, 14473 Potsdam, Germany
[3]Swiss Federal Research Institute WSL, Zürcherstrasse 111 8903 Birmensdorf, Switzerland
[4]Department of Geotechnical Engineering and Geosciences, Technical University of Catalonia UPC, Jordi Girona, 1-3 (D2) 08034 Barcelona, Spain
[5]Institute of Mountain Risk Engineering, BOKU, Peter-Jordan-Straße 82, 1190 Vienna, Austria

Received: 26 June 2015 – Accepted: 21 July 2015 – Published: 13 August 2015

Correspondence to: A. von Boetticher (albrecht.vonboetticher@usys.ethz.ch)

Published by Copernicus Publications on behalf of the European Geosciences Union.

Abstract

Here we present the validation of the fluid dynamic solver presented in part one of this work (von Boetticher et al., 2015), simulating laboratory-scale and large-scale debris-flow experiments. The material properties of the experiments, including water content, sand content, clay content and its mineral composition, and gravel content and its friction angle, were known. We show that given these measured properties, a single free model parameter is sufficient for calibration, and a range of experiments with different material compositions can be reproduced by the model without recalibration. The model validation focuses on different case studies illustrating the sensitivity of debris flows to water and clay content, channel curvature, channel roughness and the angle of repose of the gravel. We characterize the accuracy of the model using experimental observations of flow head positions, front velocities, run-out patterns and basal pressures.

1 Introduction

Debris flows are a frequent natural hazard in mountain regions. They consist of a mixture of water, clay, sand and coarser material traveling as a partly fluidized mass through steep channels. The mix of different materials leads to a complex rheological behavior that is still not well understood. Field observations of debris-flow behavior and rheology are challenging and still rare, and numerical modeling is often the approach of choice when assessment of debris-flow behavior is needed for planning, zoning, and hazard assessment (Scheuner et al., 2011; Christen et al., 2012). Most models require direct calibration to capture site-specific behavior. However, reliable calibration data are rare, and laboratory experiments cannot be perfectly scaled to field situations. In von Boetticher et al. (2015), a new solver was presented, designed for the simulation of debris flow behavior based on a single free model parameter. The model separately treats the three important phases – air, fluid, and granular material – and allows mixing

GMDD
8, 6379–6415, 2015

of the latter two. The local rheology is obtained from a linearly weighted average of the rheological properties of these two phases. Material properties are related to the fractions of different minerals within the debris-flow material.

The object of this study is to illustrate the model's capability to accurately account for the wide range of flow behaviors without recalibration. The key elements of the model concern its sensitivity to water content, gravel- and clay-fraction and clay-mineralogy on the one hand, and the interaction between the three-phase rheology and the complex three-dimensional flow structure on the other. We present the validation and limitations of the model set-up based on simulation results for intermediate and large-scale experiments.

2 Model validation and performance based on selected flume experiments

The model is based on an adaptation of the interMixingFoam solver of the open source Finite Volume Code OpenFOAM (OpenFOAM-Foundation, 2014), in combination with a stable implementation of the pressure-dependent rheology model of Domnik et al. (2013) to describe the gravel phase as a Coulomb-viscoplastic fluid, and a Herschel–Bulkley rheology implementation for the interstitial slurry of water and fine sediment. In addition to the common user-determined parameters (density, water content and relative amounts of gravel and clay), the user is required to input the clay composition, (e.g., the fractions of kaolin and chlorite, illite, montmorillonite Yu et al., 2013), and the friction angle δ of the gravel as its angle of repose. The only free model parameter used for calibration is τ_{00}, which acts as a restricted multiplication factor for the calculated yield stress of the fine sediment suspension and has been found to depend on the mesh resolution.

Three different experimental cases were chosen to illustrate how the model represents the sensitivity of the flow and deposition process to water- and clay content, channel curvature and bed roughness based on the calibration of a single free model parameter.

GMDD
8, 6379–6415, 2015

The first two sets of experiments were performed using intermediate-scale flumes at the Swiss Federal Research Institute WSL, Switzerland. The first case study includes flume experiments simulating hillslope debris flows that differ in water content but are otherwise similar. The flume was wide enough that the flow did not touch the side-walls. Thus these experiments exclude side-wall effects that may otherwise dominate the flow behavior of relatively shallow flows (Jop et al., 2008). We use this case study to illustrate that the calibrated model can predict flow behavior with different water contents without recalibration.

The second experimental case used for validation was designed to study the sensitivity of debris flows to channel curvature (Scheidl et al., 2015). The channel had a half-circular cross-section and was composed of two curves with different radii. Because debris flow material is more sensitive to curvature than Newtonian fluids in terms of surface super-elevation (lateral difference in flow surface elevation in a channel bend), this experimental set-up is suitable for verifying the modeled non-Newtonian rheology of the mixture and its dependency on local pressure.

While the two sets of experiments described above were performed with small amounts of sediment, over short times and at a laboratory scale, we also tested our model against data from full-scale experiments performed in the USGS experimental debris-flow flume at the H. J. Andrews Experimental Forest, Oregon (Iverson et al., 2010). In those experiments, debris flow material was released into a 2 m wide and about 75 m long flume with 31° inclination, followed by a smooth transition into a planar run-out area with a 3° slope in the flow direction. In the initial experiments, the channel was a flat concrete bed; in later experiments, the bed was paved with 1.6 cm high bumps. The smooth channel experiment included a sediment mixture with 2.5 times more loam than the so-called SGM mixture (Iverson et al., 2010) that was applied on the rough channel. Thus, the two subsets of experiments differ both in channel roughness and in the fraction of fine sediment.

The model setup and performance for all three cases are described in more detail in the following sections.

GMDD
8, 6379–6415, 2015

2.1 Experimental validation of water content sensitivity

In our modeling approach, the rheology of the slurry phase depends on its yield stress, which is known to be exponentially dependent on water content (e.g., Hampton, 1975; O'Brian and Julien, 1988; Yu et al., 2013; Hürlimann et al., 2015), with increasing exponents for higher clay fractions. Therefore, for each material composition there should be a critical range where a minor variation in water content causes a strong change in flow depths and run-out distance. Three experiments from Hürlimann et al. (2015) were selected, lying within the range of high water-content sensitivity. These debris-flow experiments were carried out by releasing 0.01 m^3 of debris flow material from a 0.4 m wide reservoir into a 4.4 m long and 2 m wide, 30° inclined plane followed by a 2.5 m long, 2 m wide and 10° inclined run-out section (Fig. 1). The flume was covered by a rubber layer with a burling consisting of flat circular discs of 4 mm diameter and about 0.3 mm height every 5 mm to increase roughness. The experimental sediment mixtures used for model validation only differed in water content (27.0, 28.5, and 30.0 % by weight) and contained about 1.6 % smectite, 8.8 % other clay minerals, 27.8 % silt, 47.7 % sand and 14 % gravel. The corresponding bulk densities were 1822, 1802 and 1722 $kg\,m^{-3}$.

All selected experiments were simulated using the same value of $\delta = 36°$ for the angle of repose of the gravel mixture. This friction angle was determined in a simple adaptation of the method of Deganutti et al. (2011) by tilting a large box with loose material until a second failure of the material body occurred. The model parameter τ_{00} was calibrated to fit the observed run-out length of the 28.5 % water content experiment, and the two tests with 1.5 % higher or lower water content were used to validate the sensitivity of the model to water content.

The model adapts to a new water content by calculating a new Herschel–Bulkley yield stress. However, the free model parameter τ_{00} should be adapted to the new water content, too. Let $\tau_{\text{y-cal}}^{\text{w-new}}$ be the Herschel–Bulkley yield stress calculated by the model for a new water content, but based on the original value of the calibration parameter

GMDD
8, 6379–6415, 2015

$\tau_{00\text{-cal}}$ that is not yet adjusted to the new water content. Due to the need to account for the influence of a different water content on the free model parameter τ_{00}, some user action is necessary. The free model parameter τ_{00} is reduced or increased according to equation

$$\tau_{00} = \tau_{00\text{-cal}} \frac{\tau_{\text{y-cal}}^{\text{w-new}}}{\tau_{\text{y-cal}}}, \quad (1)$$

to obtain a rheology with all parameters adapted to the new water content, where $\tau_{00\text{-cal}}$ and $\tau_{\text{y-cal}}$ denote the free model parameter value and the corresponding Herschel–Bulkley yield stress calculated by the model in the calibration test. This way, the change of the yield stress initially calculated by the model is also applied to the free model parameter.

Based on the calibrated value of $\tau_{00} = 41.33$ Pa for an experiment with 28.5 % water content (the calibration test), the rheologies of the two mixtures with 1.5 % higher or lower water content were calculated using Eq. (1). For a water content of 27.0 % (subsequently denoted as reduced water experiment) this procedure resulted in $\tau_{00} = 51.76$ Pa, whereas for the 30 % water content (denoted as increased water experiment in the following) the result was $\tau_{00} = 21.29$ Pa. For each of the three experiments, laser-measured flow depths were available in the center of the flume, one meter downslope of the gate. Comparisons between measured and simulated flow depths at such small scales are only approximate due to the surface disturbance by coarser grains that cause significant fluctuations in surface elevation. However, the arrival time, the maximal flow depths and the decay of surface elevation over time were considered to be suitable for comparison to the model. The model performance was evaluated by comparing the deposition patterns, travel times, and time series of flow depths in the simulations and experiments. The simulated flow depths reproduce the laser signal with respect to both time and amplitude (Fig. 2) and predicted run-out deposits replicate the water content sensitivity (Fig. 3). Although the front arrival of the reduced water test is delayed by 0.2 s in the simulation, the maximum flow depth is reached at the same time

GMDD
8, 6379–6415, 2015

in the experiment and simulation (Fig. 2 top). The maximum flow depth is accurately predicted by the model, with a deviation of 2 mm, which is less than the average gravel grain size. The fast decrease of the measured surface elevation within 0.1 s after the peak is well captured by the model, followed by a moderate decrease until 1.2 s. At this point, in the experiment a transition began towards the stable level of about 11 mm flow depth, which corresponds to the maximum grain size. This transition begins later in the simulation and declines further to a modeled final deposit of 6 mm thickness; however, large measured fluctuations of flow depth are likely due to the coarser grains present in the test. The predicted deposit length of 2.42 m in the simulation overestimates the experimental value of two meters (Fig. 3 top). However, the simulated front also temporarily paused at $x = 2.04$ m, until it was overrun by a second wave 0.1 s later. There is an almost perfect fit between the shapes of the experimental and simulated deposits in the calibration case (Fig. 3 center). The maximum flow depth and the subsequent decrease are well reproduced (Fig. 2 center), although the front arrival time at the laser is again delayed by some 15 %. The measured and simulated flow depth in the wet experiment show that the early front arrival time and the time of the maximum flow depth are precisely predicted by the model. The moderate decrease of the surface elevation over time is captured by the model (Fig. 2 bottom), although the maximum flow height is underestimated. The final deposit thickness of about 4 mm at the laser is reproduced correctly but the run-out length of 5.17 m is over-predicted by about 7 % compared to the experimental value of 4.84 m (Fig. 3 bottom).

2.2 Non-Newtonian rheology in channel curvature: evaluation of increased surface super-elevation due to curvature

Enhanced super-elevation due to curvature is characteristic for viscous debris flows (Wang et al., 2005; Bertolo and Wieczorek, 2005), so it can be viewed as a further indicator for model quality in our case. As we expect the enhanced super-elevation of debris flows in curved channels to be connected to a change of viscosity due to the pressure increase caused by deflection within the curve, the second group of ex-

GMDD
8, 6379–6415, 2015

periments focuses on the pressure-dependent rheology. A correct representation of super-elevation of deflected material by the model would suggest that the interplay between pressure- and shear-rate-dependent viscosity is handled correctly. With β as the average surface inclination transverse to the flow direction, a correction factor k^* can be defined as the ratio between the gradient of super-elevation $\tan(\beta)$ of debris flow material and the corresponding gradient of clear water with the same average flow velocity. Based on the forced vortex approach with the assumption of a constant radius of the channel bend, Scheidl et al. (2015) analyzed the influence of viscosity and the boundary effects in bends for debris flows and back-calculated correction factors for a number of flume experiments.

The experiments were performed by releasing 0.0067 m^3 of material from a reservoir, through a transitional "box-to-channel" reach, into a channel of half-circular cross-section with 0.17 m diameter and a constant downslope channel inclination of 20° (Scheidl et al., 2015). The channel was arranged in an S-shape, with a first 60° curve to the left with 1.5 m curve radius followed by a second curve to the right with 1 m curve radius (Fig. 4). The channel was covered with sandpaper to increase roughness.

Here, we consider the mixture with the largest clay content (mixture A, Scheidl et al., 2015) where less demixing and phase separation was observed, and focus on the first curve of 1.5 m radius. The flow height in a cross section, two-thirds of the way through the curve, was measured by three lasers across the channel (Fig. 5). The arrival time at the laser section could not be used as a criterion for model calibration, because a simplification of the box-to-channel reach was necessary. This was due to the fact that the complex geometry at the transition to the channel (Fig. 4 region d) caused local air inclusions. A very fine grid resolution would be necessary here to adequately simulate the immediate demixing of the air. Therefore, as a simplification in our model set-up, the straight channel section was extended to the reservoir where it was filled with material at rest. Thus, measured travel times between the gate and the first lasers are not comparable to the model. Instead, the free model parameter was calibrated to correctly predict the front velocity at the laser section. This front velocity was determined from

GMDD
8, 6379–6415, 2015

high-speed video recordings. The average value from all experiments with mixture A at the upper curve was 1.49 m s^{-1}, leading to τ_{00} = 26 Pa to reach the same flow front velocity in the simulation. Mixture A was composed of 6.5 % clay, 15 % silt, 26.1 % sand and 52.4 % gravel by dry weight. Since the gravel phase in the experiment was created from the same gravel as used in Sect. 2.1, a value of $\delta = 36^{\circ}$ was applied here, too. The water content was 27 % and the density of the mixture was about 1800 kg m^{-3}.

The measured and simulated surface deflections can be compared to assess how well the modeled rheology accounts for the increased super-elevation. Nevertheless one should be aware that in this experimental setup, a granular front developed, which is in contradiction to the homogeneous phase distribution in the current implementation (Fig. 5 right). The laser at the inside of the curve did not always register any material in the experiments or simulation, so the gradient of the super-elevation angle, tan(β), is reconstructed from the simulation once as tan(β_{max}) by using the points of maximal surface elevations at the inside and outside of the flow (P_i and P_o in Fig. 5), and once as tan(β_{min}) based on the elevations of laser 2 and laser 3. At the moment of maximum surface elevation, the modeled tan(β_{max}) equals 0.336 resulting in $k^* = 2.11$ as defined in Scheidl et al. (2015), which fits the experimental average of 0.33 (Scheidl et al., 2015, Table 2) and the correction factor $k^* = 2.1$. The corresponding value for tan(β_{min}) reaches 0.243, underestimating the experimental values, however, the corresponding correction factor k^* equals 1.52 and still lies within the experimental standard deviation. The surface super-elevation is captured by the model although the front volume is underestimated by more than 50 %. The under-predicted volume is a consequence of both the simplified geometry of the release area and from a continuous over-prediction of material lost at the channel margins due to the no-slip boundary condition, whereas in the experiment little material was deposited at the wall because the walls were moistened prior to the experiment. This problem needs to be addressed before more detailed comparisons can be made. Nevertheless this example is included to illustrate that the model can predict plausible superelevation.

GMDD
8, 6379–6415, 2015

2.3 Large scale experiments: effects of bed roughness and share of fine material

Since it is difficult to upscale from laboratory-scale tests to true debris flow events, large-scale debris flow experiments are essential for model validation. The USGS debris-flow flume consists of a 75 m long, 2 m wide and 31° inclined concrete channel, with a release reservoir having the same width and slope, and an approximately 7.5 m long distal reach where the bed inclination forms a smooth transition to a run-out plane with a 2.5° inclination and no lateral confinement (Iverson et al., 2010). Laser rangers measure the flow height 32 and 66 m downslope from the release gate, and a third laser is located in the run-out plane. The flume is tilted to one side, and the maximum tilt reaches 2°. The model accounts for this with a 1° tilt over the whole flume length.

We selected two experimental setups. One focused on the rheology of the muddy suspension, so we chose an experiment with high content of loam and a smooth channel bed surface, to reduce the influence of granular collisions. A material mixture of 5.25 % clay, 12.25 % silt, with 32 % sand and 50.5 % gravel by dry weight was applied. The water content and density of this test were determined as 20.6 % of mass and 1920 $kg\,m^{-3}$ by assuming fully saturated material. The other setup should illustrate the interplay with the gravel, so a rough channel bed was used and the released material consisted of the so-called SGM mixture Iverson et al. (2010), which is composed of 2.1 % clay, 4.9 % silt, with 37 % sand and 56 % gravel (by dry weight). The SGM mixture has 17.9 % water content and 2010 $kg\,m^{-3}$ density (based on Iverson et al., 2010, Table 2). According to James and Bait (2003), we assume that kaolinite dominates the clay minerals, although smectite could be present. The angle of repose was estimated on the basis of tilt table tests of the sand and gravel mixture as 39.6° (Iverson et al., 2010, see column (SGM) in Table 3).

An important element of our simulation is that we compare the model with the rough channel experiments based on the calibration of the smooth bed experiment that con-

GMDD
8, 6379–6415, 2015

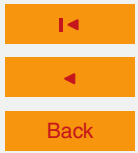

tained 2.5 times more loam and 2.5 % more water in the material mixture. This way we aim to illustrate that the calibrated model can predict the flow process of a different mixture in a channel with different bed roughness. The detailed analysis of the model performance for the rough and smooth channel experiments highlights this in the following.

2.3.1 Smooth channel experiment with high content of loam

In test 970722 (numbering as YYMMDD), the channel bed consisted of smooth concrete. Only video documentation is available (Logan and Iverson, 2013), limiting the detail of comparison between simulation and experiment. The model parameter $\tau_{00} = 90$ Pa was calibrated such that the time between release and front arrival at the run-out plane matches the experiment (Fig. 6). Both the run-out process and the final deposit therefore contribute to the model validation, since they were not considered for the calibration. The simulated spreading into the run-out plane evolves in good agreement with the experimental observations (Fig. 7 top). A slight irregularity at the right side of the front forming a shoulder is also captured by the model. After 8.2 s, simulation and experiment both reach 14 m run-out distance. The simulated front is still pushed by the fast material that follows from the debris flow tail with surface velocities of more than 8 m s^{-1}, whereas the corresponding experimental material has surface velocities of about 2 m s^{-1} (Fig. 7 bottom). In the experiment, a second large surge arrived at the run-out plane after the time sequence shown in Fig. 7, overran the immobile deposit and widened the material deposited at the foot of the channel. By contrast, the model evolves in a single surge and the modeled material front propagates about 1.5 s longer until it reaches 18.5 m, overestimating the run-out length by about one third. The maximum deposit length on the run-out plane in the experiment was 14 m and the simulated front reached that point at the same time as the flow front in the test.

GMDD
8, 6379–6415, 2015

2.3.2 Rough channel experiment with small content of loam

For the rough channel experiments, round bumps of 1.6 cm height were installed on the bed every 5 cm; these were introduced in the model as pyramids (Fig. 8). Flow depth and basal force measurements were available as averaged values over a set of experiments with identical release and channel setup, where the SGM material mixture (Iverson et al., 2010) containing 2.1 % clay, 4.9 % silt, with 37 % sand and 56 % gravel (by dry weight) forms a 9.7 cubic-meter release body of known geometry. Three SGM experiments published by Iverson et al. (2010) with different flow front velocities were selected for front position comparison. The test from the year 2000 represents an extreme case with a quite low front velocity in the beginning followed by a sudden speedup of the flow front after 6 s. The other two tests also show a sudden acceleration of the flow front, but their release process was faster and the sudden change in front velocity appeared later and was less dominant (Fig. 10). To some extent the difference in front position over travel time seems to be due to a large second surge that originates from the reservoir (Fig. 11). Especially in test 000928, part of the material left the reservoir with a delay, but as the second surge arrived at the front, the material front velocity doubled from about 8 to 16 $\mathrm{m\,s^{-1}}$.

The calibrated value of $\tau_{00} = 90$ Pa obtained from the smooth channel experiment was applied without any adjustments to model the rough channel experiments with the SGM mixture by using Eq. (1), resulting in $\tau_{00} = 82.78$ Pa. Because the grid resolution changed to represent the bumps on the channel bed by pyramids, the value for τ_{00} is not expected to be precisely correct, but satisfactory to illustrate the model's capability to account for different mixtures and channel geometries without recalibration. The average friction angle of the sand and gravel mixture was applied. In addition, a second simulation with a friction angle corresponding to the lower limit of measured friction angles was carried out. In this way, while keeping the value of the lower friction angle within the range of realistic values, we intend to balance out the overestimated roughness of the half-spherical bumps by their modeled representation as pyramids. Both

GMDD
8, 6379–6415, 2015

simulation results, i.e. $\delta = 39.6^{\circ}$ and $\delta = 36.6^{\circ}$, are shown in the diagrams to demonstrate that the effect is relatively small.

Flow front position, shape and surface wave patterns (derived from video recording) were compared to the corresponding simulations (Figs. 10 and 12), indicating a good agreement in front position and a comparable pattern of the small surface waves. The simulation with reduced gravel friction angle shows better agreement in the decelerating part of the flume, as expected. In the upper part of the flume, the modeled front seems to proceed too fast, which is expected due to the neglected gate opening process. However, a comparison of the modeled flow depths with the ensemble-averaged laser signal from all eight published SGM experiments 32 m downslope from the release gate shows that the simulated front arrives just in time (Fig. 13). The flow depths develop over time in general within the standard deviation range of the measured values at that point, except at the late tail of the flow after 8 s from release, where both simulations result in some overestimation corresponding to two slow surface waves passing. The simulation with the smaller friction angle of $\delta = 36.6^{\circ}$ reduces the oscillation of flow depths compared to the simulation with the larger gravel friction angle. The measurements of three force plates installed at 31.7, 32.3 and 32.9 m were averaged over all twelve SGM experiments and compared with the pressure in the corresponding cells of the simulation (Fig. 14). In the simulations, the pronounced oscillation of modeled basal pressure underneath the fast front exceeds the range of the measurements.

3 Discussion

This study represents an attempt to develop a widely applicable modeling framework for debris-flow simulations, based on rather simple constitutive equations describing the two-phase flow rheology and combined with traditional 3-D CFD modeling. Nevertheless the results are surprising, as it appears to be possible to produce accurate front velocities, flow depths and run-out distances after calibration of a single model parameter. Furthermore, the results show that the model can accurately simulate de-

GMDD
8, 6379–6415, 2015

bris flow behaviors that differ by more than one third in travel time or run-out distance without recalibration, just by taking into account the local channel topography and differences in material properties such as clay, sand and gravel composition, as well as water content.

The simulations of the small-scale experiments that focus on water content sensitivity could reproduce the pronounced dependency of the run-out length on water content. The model could to predict flow depth developments over time. Some short-time peak deviations between observations and simulations reached values close to the maximum grain size, possibly resulting from single grain effects. A slight overestimation of the influence of the higher water content led to a run-out over-prediction by 7 % in the model compared to the observation. The deposit of the calibration test case was accurately reproduced by the model, but the run-out of the reduced water content experiment was over-predicted by 21 %. This discrepancy might be reduced with better grid resolutions, because the simulated front for the reduced water content experiment came to a halt at the correct position but was overrun by a second pulse of material, leading to an unrealistic air inclusion within the simulated front. The absence of discrete particles in the model allows the second pulse to pass over the front without any roughness elements. The same limitation by grid resolution and by the absence of particles becomes apparent when looking at the simulated run-out tip of the experiment with increased water content. Due to the large stretching of the material, the flow front depth was represented by less than five grid cells, resulting in an inaccurate velocity profile and shear gradient, and thus leading to an imprecise viscosity. Furthermore, the interface thickness of the Volume Of Fluid approach at such low grid resolutions in relation to flow depth leads to significant air phase concentrations over the whole flow depth of the front. This results in a reduced density and viscosity at the flow front.

The results of the curved channel experiments are encouraging. If the superelevation of the surface due to channel curvature can be represented with such accuracy for the true flow front volume, other mixtures and the lower channel bend, it would represent strong evidence for an adequately modeled interplay between gravel

GMDD
8, 6379–6415, 2015

and slurry rheology. The focus on a mixture of high clay content was due to the fact that our simplified solver cannot account for phase separations due to grain-size sorting. The upper curve was chosen to save computational time. However, the non-Newtonian behavior resulting in increased super-elevation was more pronounced for mixtures with less clay content and slower front velocities at the lower curve. Although we did not consider the experimental flows in the lower curve, we can expect an enhanced influence of the pressure in the model at the lower curve, because the slower flow has a reduced shear gradient compared to the upper curve flows. From the results obtained at the upper curve, we may at least conclude that the model can reproduce enhanced super-elevations and seems to be suitable to predict debris-flow breakouts in curved channels for hazard assessment. The main limitation is that the maximum cross-sectional area of the simulated flow reaches only about 40 % of the area determined from the experiments. We severely underestimate the debris flow volume at the curve due to the simplified release geometry and due to material losses to the walls in the model by the no-slip boundary condition. Therefore, an improved mesh including the reservoir and the box-to-channel reach is necessary before addressing the flow in the lower curve, which is beyond the scope of this paper.

The large-scale experiments at the USGS flume were chosen as examples of flows closest to prototype conditions of the real world, with relatively small uncertainties concerning material composition, flow front velocity or run-out patterns. The experimental flow behavior was well captured by the model. In particular, the model successfully adapted without recalibration to a material mixture containing 2.5 times less loam, combined with a severe change of channel roughness.

For the smooth channel bed, a good representation of the travel time and front shape on arrival could be achieved. The spreading into the run-out plane was examined in detail. In both the experiment and the simulation, the front arrived at the experimental maximum deposit length at the same time with accordant positions and front shapes at intermediate time steps. This indicates that the model captures the deceleration process with high precision. However, the modeled material front did not come to a halt,

GMDD
8, 6379–6415, 2015

but instead continued, such that the maximal deposit length was over-predicted by about one third. The reason for this deviation is probably the over-predicted material volume following the front, which arises from the modeled flow process as a single surge event. Because the material in this smooth channel test flowed in two separate surges, less material was present in the physical experiment to catch up with the front which led to reduced inertia and deposit length compared to the single surge model. According to video recordings of the released material in the reservoir, we infer that the second surge originated from the reservoir in analogy to the second surge in the rough channel experiments. Besides run-out distance, the model captures the different character of the sides of the material front, with one side smooth and the other side irregular. This is due to the sensitivity of the debris flow to the slight lateral tilt of the flume of up to 2 % and the detailed run-out pad topography (Iverson et al., 2010) that were included in the model.

A key result of the large-scale tests is the capability of the model to predict the much slower flow-front velocity of the rough channel experiment based on a calibration for a smooth channel and a mixture of 2.5 times higher content of loam. Three experiments of identical setup using the so-called SGM mixture together with a rough channel bed were selected to compare flow front velocities with the simulation. Ensemble-averaged time evolutions of flow depths and basal pressures of twelve such experiments were compared to the model output. The simulated flow depths lie in general within the range of standard deviations of the measurements. However, considering the basal pressures, part of the deviations between experiment and simulation may arise from the pyramid representation of the half-spherical bumps in the rough channel bed, leading in the model results to overestimated pressure peaks and thereby to an exaggerated viscosity by the pressure-dependent gravel rheology. A reduced friction angle therefore improved the modeled flow front velocity, although the effect is not visible in the basal pressure fluctuation. Because grain-size sorting effects and the release mechanism are not accounted for, a single surge flow forms in the simulation, in contrast to the real tests with two surges as in most of the experiments considered. Therefore, when the

GMDD
8, 6379–6415, 2015

modeled debris flow reaches the end of the channel, the front composition and volume is not an adequate representation of the experiment. As a consequence we did not model the run-out patterns of the rough channel experiments, in contrast to the smooth channel experiment where less demixing occurred.

On the one hand, it might be possible to obtain better representations of all SGM experiments with the current model by varying τ_{00} or density, water content, or the friction angle within the range of the published standard deviations of the experimental setup. On the other hand, we preferred to illustrate the model reliability based on input derived from averaged measurements to avoid unrealistic expectations that can not be fulfilled in practice. To alter the level of detail, it would be more appropriate to include grain-size sorting effects and the release mechanism of the bouncing gate before approaching each individual test with test-specific parameters.

Among other models applied to the SGM experiments, George and Iverson (2014) recently performed simulations with the depth-averaged two-phase model of Iverson and George (2014). The model uses a bulk drag between grains and interstitial fluid based on Darcy's law together with a description of the dilatancy angle and takes into account the excess pore fluid pressure p_e described by a forced advection–diffusion equation

$$\frac{\mathrm{d}}{\mathrm{d}t}p_e - \frac{k}{\alpha_m \mu}\nabla^2 p_e - \frac{1}{\alpha_m}\left[\nabla\frac{k}{\mu}\right]\cdot\nabla p_e = \frac{\mathrm{d}}{\mathrm{d}t}\sigma - \frac{\dot{\gamma}\tan\psi}{\alpha_m}. \quad (2)$$

Here, α_m is the debris compressibility depending on the material composition and solid fraction, k is the hydraulic permeability of the granular aggregate, which depends on a model parameter and the solid fraction, ψ is the dilatancy angle (which depends on the solid fraction, the shear-rate, the viscosity, and on a stress and density-dependent local equilibrium of the solid fraction), σ is the local stress reduced by hydrostatic pressure, and μ and $\dot{\gamma}$ denote viscosity and shear rate. Besides the simplifications involved by depth-averaging Eq. (2), the model is also limited by the assumptions of Newtonian viscosity, a shear rate assuming simple homogeneous shearing, and a fixed grain-size-independent length scale within the dilatancy formulation (which accounts for the

GMDD
8, 6379–6415, 2015

generation of normal stresses by grain collisions during shearing). The pore fluid pressure is used to decrease basal Coulomb friction whereas the dilatancy angle is added to the basal friction angle. In this context, it is interesting that the smooth basal lithostatic reference pressures generated by the calibrated model for the SGM experiments exceed 3 kPa at a position 32 m downslope from the gate (George and Iverson, 2014). Against this background, the corresponding strong basal pressure oscillations in our model seem to be reasonable given the fact that we model incompressible flow. It may be of interest how the dilatancy model would evolve if the vertical momentum exchange and the detailed channel roughness would be included. Besides the need to account for grain-size sorting as the next step, we highlight the sensitivity of the debris flow event to the gate opening. We performed simulations of the gate opening process; these simulations support the findings by George and Iverson (2014) showing that the gate opening influences the flow front. With respect to the phenomenon of a second surge, the observed bounce-back of the gate might play a role as well. However, we aim to address this issue together with the grain-size sorting process in a follow-up study.

Our approach allows the model parameters to be linked to material properties and local topography. It suggests that one should be able to develop a model that can be applied to a wide range of debris-flow simulations, wherever the necessary data on material and site conditions are available. The purpose was not to gain a perfect representation of the experiment, but to see how the chosen rheology represents the sensitivity to water content, channel roughness and curvature, and fraction of fine material. The new model overcomes a weak point of debris flow modeling: debris flow models commonly depend on many free parameters or are simplified by either modeling the flow from a granular perspective neglecting the interstitial fluid, or as a viscous continuum without accounting for the granular component of the flow process. Two-phase approaches, on the other hand, come along with high numerical costs. In case of two-phase coupling by drag between grain and fluid, the uncertainty in the drag between granular and fluid phases brings along parameters that are difficult to quantify in case

GMDD
8, 6379–6415, 2015

of the non-Newtonian suspension and non-spherical gravel grains. As a consequence, no previous modeling approach succeeded in predicting debris-flow behavior across such different experimental settings as those examined here, with modifications to only a single parameter. Beyond that, our model succeeded in simulating different material mixtures without recalibration. However, numerical costs are still high for accurate results. The application is suitable for situations where the detailed flow structure is required. While the simulation of the smooth channel debris flow experiment at the USGS flume required seven hours per second of flow using 32 processors on the WSL Linux cluster HERA (consisting of Six Core AMD Opteron 2439 at 2.8 GHz), the rough channel experiment demanded ten hours per second of simulated flow and 44 processors due to the high grid resolution. However, these estimates are conservative because we did not have exclusive use of the cluster during these tests.

4 Conclusions

We demonstrated the wide range of applicability of our new numerical debris-flow model. The model concept follows the strategy of shifting from requiring user expertise in debris flow model calibration towards requiring information about the modeled site. The presented simulations of a wide range of different experiments lead to the following conclusions:

1. The material mixture can be characterized based on clay mineral composition, content of clay, silt, sand and gravel, angle of repose of the gravel, and water content. A single free parameter allows calibration to adjust the model to the grid resolution.

2. The model can account for changes in the material mixture without recalibration.

3. The model can account for the sensitivity of the rheology to channel geometry, including the enhanced surface super-elevation of debris flows in curved channels.

GMDD
8, 6379–6415, 2015

4. The sensitivity to surface roughness is captured by the model and it can be varied without recalibration.

The need to calibrate only a single parameter greatly simplifies the model calibration process. This can save significant time while still providing a model of high detail and reliability. Although such a minimally parameterized model may fit the real-world data less well than a highly parameterized model (perhaps because the latter is over-fitted), the time saved in calibration can be used to explore a wider range of material composition and site properties. Because such changes in model setup are translated into consequences for the flow physics by the model, the ensemble of such simulations may mirror how the modeled site would respond to similar changes. Recalibrated models cannot deliver such information. Furthermore, in our model there is less room for the user to make arbitrary parameter settings than in models with several calibration parameters. Thus it may be possible to quantify the model's reliability in a robust and general way, because different users probably apply comparable parameter settings. However, one missing step is the inclusion of phase separation due to grain-size sorting effects, which would not only enable simulation of the granular front but also could enhance the model's capability to perform channel bed erosion by mobilizing gravel deposits. This extension may be included in future versions of the model.

Code availability

The source-code can be downloaded from the supplement application.zip, please follow the instructions given in the README15.pdf file for installation.

The Supplement related to this article is available online at doi:10.5194/gmdd-8-6379-2015-supplement.

GMDD
8, 6379–6415, 2015

References

Bertolo, P. and Wieczorek, G. F.: Calibration of numerical models for small debris flows in Yosemite Valley, California, USA, Nat. Hazards Earth Syst. Sci., 5, 993–1001, doi:10.5194/nhess-5-993-2005, 2005. 6386

Christen, M., Bühler, M., Bartelt, P., Leine, R., Glover, J., Schweizer, A., Graf, C., McArdell, B. W., Gerber, W., Deubelbeiss, Y., Feistl, T., and Volkwein, A.: Integral hazard management using a unified software environment: numerical simulation tool "RAMMS" for gravitational natural hazards, in: 12th Congress INTERPRAEVENT, Proceedings Vol. 1, International Research Society INTERPRAEVENT, Grenoble, France, 77–86, 2012. 6381

Deganutti, A., Tecca, P., and Genevois, R.: Characterization of friction angles for stability and deposition of granular material, in:Italian Journal of Engineering and Environment: 5th International Conference on Debris-Flow Hazards: Mitigation, Mechanics, Prediction and Assessment, Padua, Italy, 313–318, 2011. 6384

Domnik, B., Pudasaini, S., Katzenbach, R., and Miller, S.: Coupling of full two-dimensional and depth-averaged models for granular flows, J. Non-Newton. Fluid, 201, 56–68, 2013. 6382

George, D. L. and Iverson, R. M.: A depth-averaged debris-flow model that includes the effects of evolving dilatancy. II. Numerical predictions and experimental tests, Proc. R. Soc., 20130820, doi:10.1098/rspa.2013.0820, 2014. 6396, 6397

Hampton, M.: Competence of fine-grained debris flows, J. Sediment. Petrol., 45, 834–844, 1975. 6384

Hürlimann, M., McArdell, W., and Rickli, C.: Field and laboratory analysis of the runout characteristics of hillslope debris flows in Switzerland, Geomorphology, 232, 20–32, doi:10.1016/j.geomorph.2014.11.030, 2015. 6384

Iverson, R. M. and George, D. L.: A depth-averaged debris-flow model that includes the effects of evolving dilatancy. I. Physical basis, Proc. R. Soc., 20130819, doi:10.1098/rspa.2013.0819, 2014. 6396

Iverson, R. M., Logan, M., Lahusen, R. G., and Berti, M.: The perfect debris flow? Aggregated results from 28 large-scale experiments, J. Geophys. Res., 115, F03005, doi:10.1029/2009JF001514, 2010. 6383, 6389, 6391, 6395, 6411

James, M. and Bait, K.: Geologic Interpretation of Floodplain Deposits of the Southwestern Willamette Valley, T17SR4W With Some Implications for Restoration Management Practices Eugene, James Geoenvironmental Services and Eugene District BLM, Oregon, 2003. 6389

GMDD
8, 6379–6415, 2015

Jop, P., Forterre, Y., and Pouliquen, O.: Crucial role of side walls for granular surface flows: consequences for the rheology, J. Fluid Mech., 541, 167–192, 2008. 6383

Logan, M. and Iverson, R.: Video Documentation of Experiments at the USGS Debris-Flow Flume 1992–2006, Website U.S. Geological Survey Open-File Report 2007-1315, v. 1.3, available at: http://pubs.usgs.gov/of/2007/1315/ (last access: 8 August 2015), 2013. 6390

O'Brian, J. and Julien, P. Y.: Laboratory analysis of mudflow properties, J. Hydraul. Eng.-ASCE, 114, 877–887, 1988. 6384

OpenFOAM-Foundation: OpenFOAM Standard Solvers, Website User Guide of OpenFOAM, available at: http://www.openfoam.org/docs/user/standard-solvers.php (last access: 8 August 2015), 2015. 6382

Scheidl, C., McArdell, B. W., and Rickenmann, D.: Debris-flow velocities and superelevation in a curved laboratory channel, Can. Geotech. J., 305–317, 2015. 6383, 6387, 6388

Scheuner, T., Schwab, S., and McArdell, B. W.: Application of a two-dimensional numerical model in risk and hazard assessment in Switzerland, in: 5th International Conference on Debris-Flow Hazards Mitigation: Mechanics, Prediction and Assessment, Padua, Italy, doi:10.4408/IJEGE.2011-03.B-108, 993–1001, 2011. 6381

von Boetticher, A., Turowski, J. M., McArdell, B. W., Rickenmann, D., and Kirchner, J. W.: DebrisInterMixing-2.3: a Finite Volume solver for three dimensional debris flow simulations based on a single calibration parameter – Part 1: Model description, Geosci. Model Dev. Discuss., 8, 6349–6378, doi:10.5194/gmdd-8-6349-2015, 2015. 6381

Wang, Z. Y., Wang, G. Q., and Liui, C.: Viscous and two-phase debris flows in southern China's Yunnan Plateau, Water Int., 30, 14–23, 2005. 6386

Yu, B., Ma, Y., and Qi, X.: Experimental study on the influence of clay minerals on the yield stress of debris flows, J. Hydraul. Eng.-ASCE, 139, 364–373, 2013. 6382, 6384

GMDD
8, 6379–6415, 2015

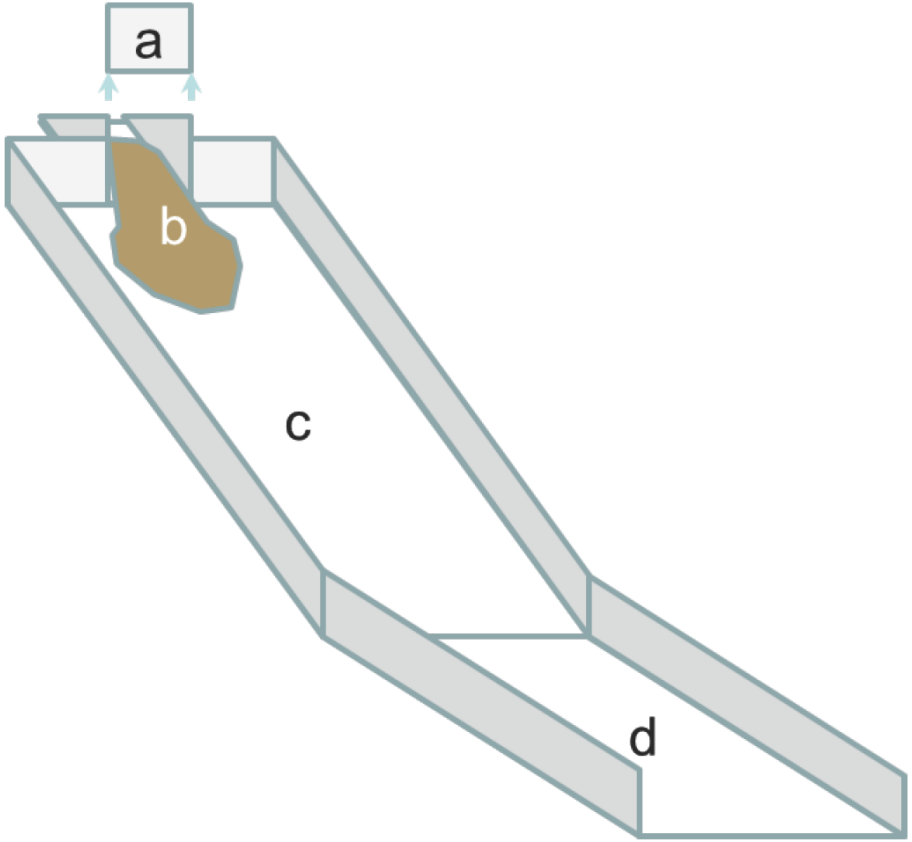

Figure 1. Iso-view sketch of the hill-slope debris-flow flume. Material (b) is released from the reservoir at the top by a sudden vertical removal of a gate (a) and flows down a steep slope (c) followed by a gently inclined run-out plane (d).

GMDD
8, 6379–6415, 2015

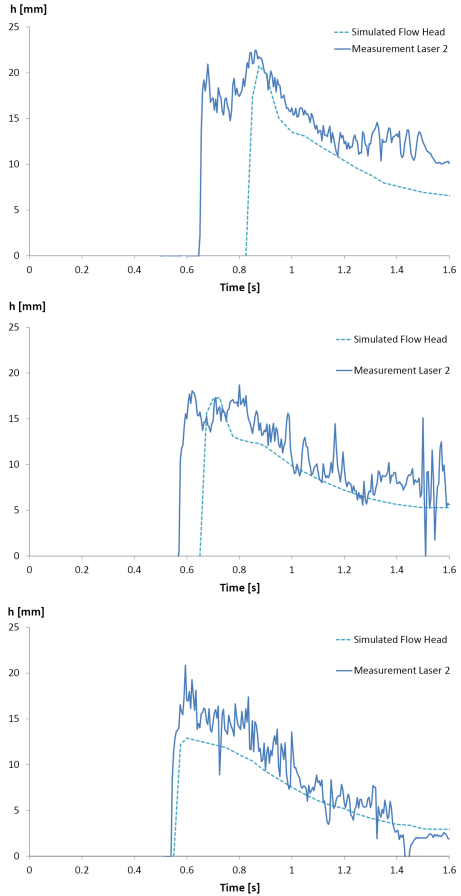

Figure 2. Laser measurement and corresponding simulated values of the flow head over time, one meter down-slope of the gate for the experiments with the water contents of 27 % (top) 28.5 % (center) and 30 % (bottom). The laser data were box-averaged over 10 ms.

GMDD
8, 6379–6415, 2015

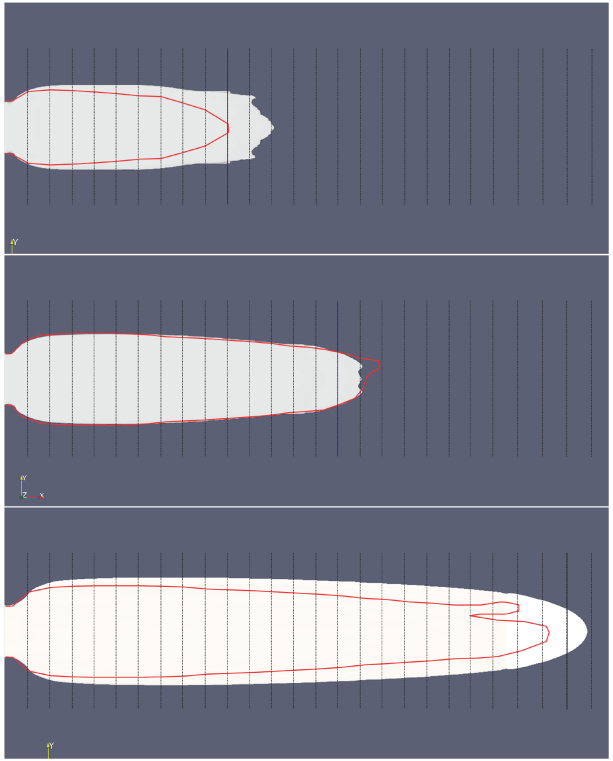

Figure 3. Simulated deposits for the mixture with 27.0 % (top), 28.5 % (center) and 30 % water content (bottom) without parameter adjustments applying $\delta = 36^{\circ}$. The thick solid lines indicate the experimental deposits and vertical thin lines represent the 20 cm spacing marks in the experimental slope.

GMDD
8, 6379–6415, 2015

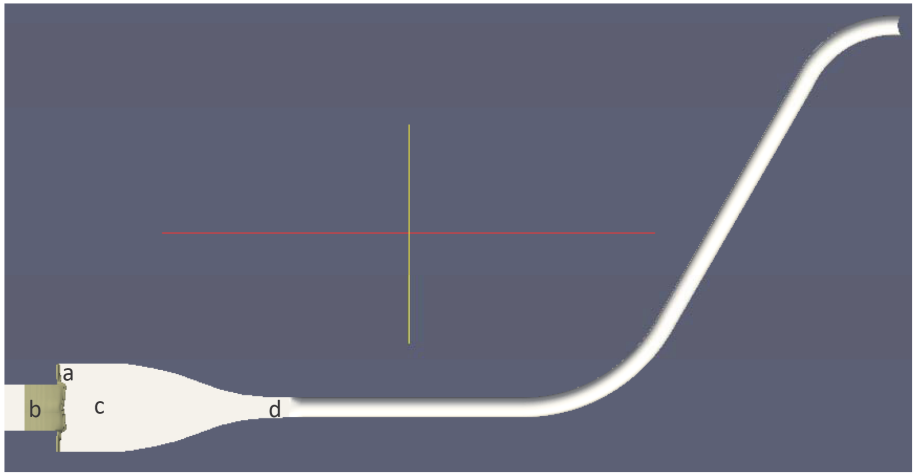

Figure 4. View from top on the modeled curved channel with release material at the reservoir (b) passing a flap gate (a) into the plane transition box (c). At the restriction (d) the channel profile changes from a rectangle to a half-pipe.

GMDD
8, 6379–6415, 2015

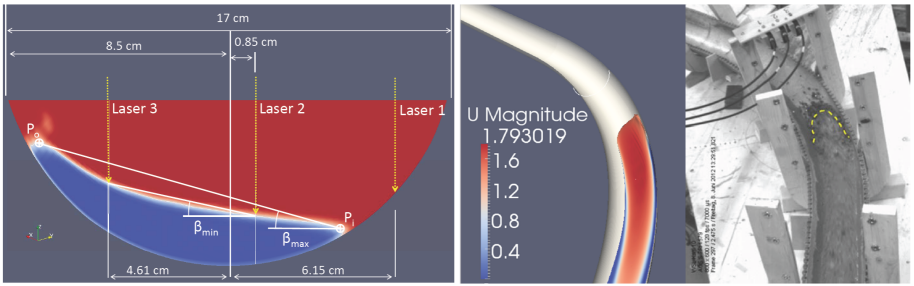

Figure 5. Left: view upstream on modeled channel section 40° after the beginning of the curve, showing air (red), debris mixture (blue), laser positions and minimal and maximal superelevation angles β. Right: screen-shot of modeled and experimental flow surface before reaching the laser section at the upper curve. The color bar denotes simulated surface velocity in [$m\,s^{-1}$], the dashed line in the experiment indicates the transition between the granular front and the viscous mixture.

GMDD
8, 6379–6415, 2015

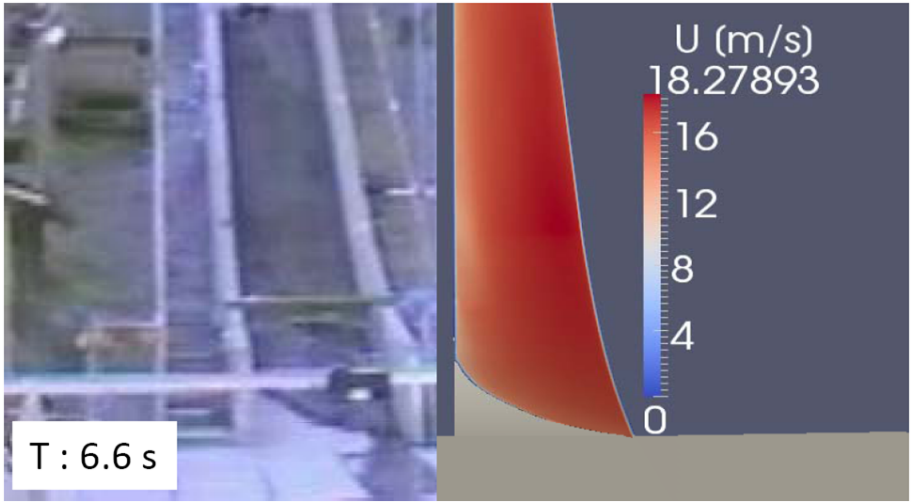

Figure 6. Observed and simulated flow front at the end of the channel for a smooth channel bed and high content of loam. The free model parameter τ_{00} was calibrated to 90 Pa to gain an identical arrival time in experiment and simulation. The simulated time was measured from the moment of release and the corresponding experimental time was derived by counting the number of video frames in the overview camera video between release and arrival in the run-out plane.

GMDD
8, 6379–6415, 2015

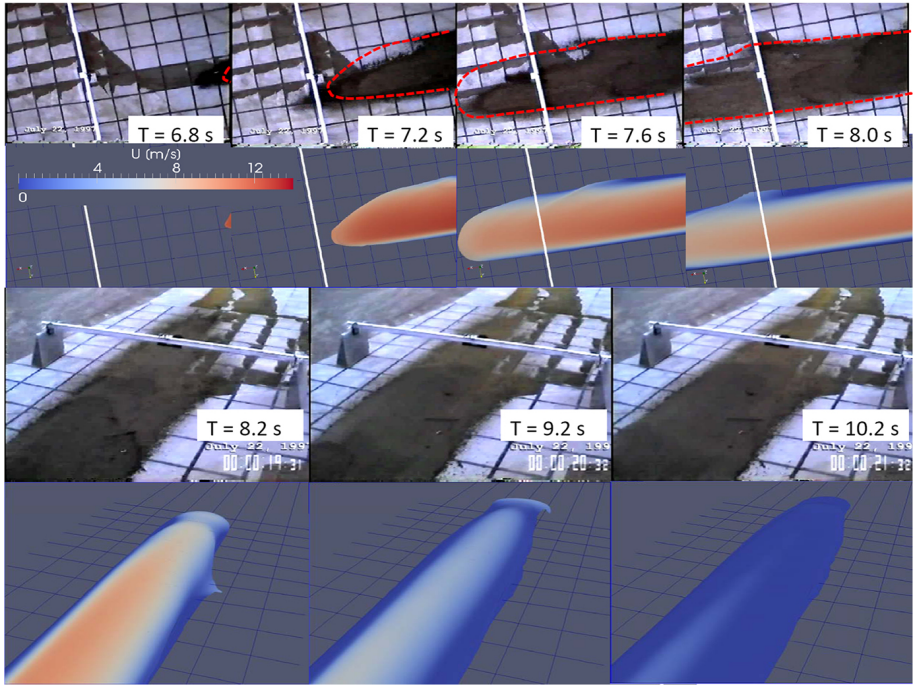

Figure 7. Time-tracking of the run-out process by top camera (upper rows) and iso-perspective camera views (lower rows). The corresponding simulated material is colored by flow velocity and the shape of the simulated run-out is copied into the camera pictures as a dashed line for better comparison.

GMDD
8, 6379–6415, 2015

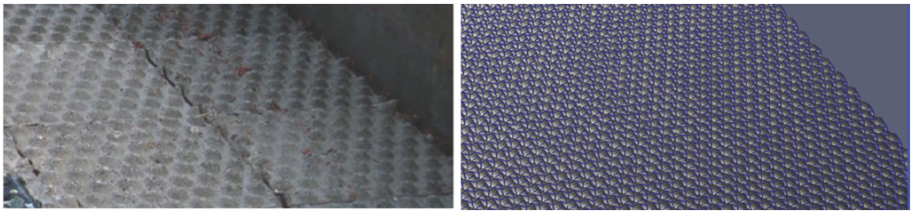

Figure 8. Perspective selection of the rough channel bed at the experimental site (above) and in the simulation (below). Transverse to the flow, a higher number of bumps was introduced into the model, which allowed to combine simple meshing with a high resolution for transversal flows.

GMDD
8, 6379–6415, 2015

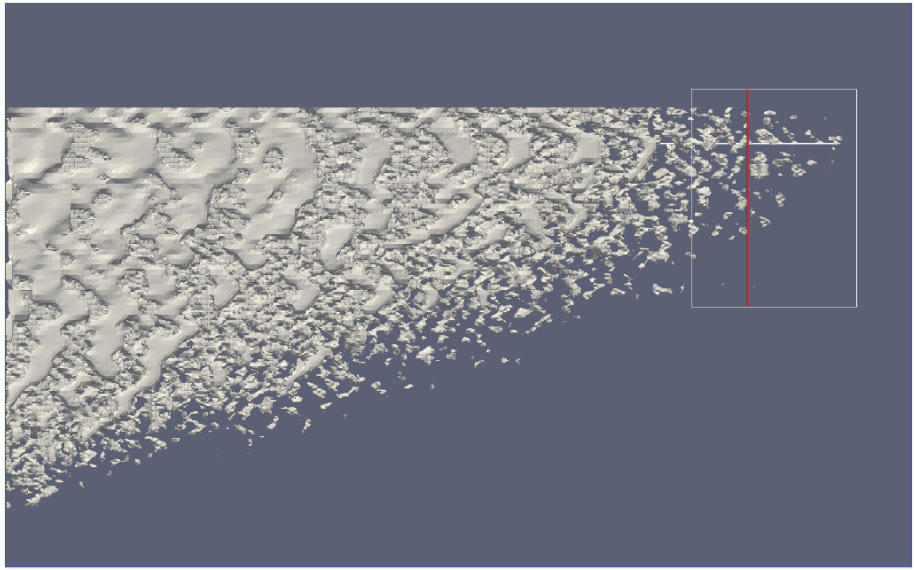

Figure 9. Top view of the modeled flow front, with the transition between air and debris flow material, marked here by the layer with material concentration equal to one third, shown as a free surface. The vertical bar (red) within the white rectangle marks the flow front position presumed as the beginning of the continuous surface, with the purpose to neglect single drops that may spread ahead.

GMDD
8, 6379–6415, 2015

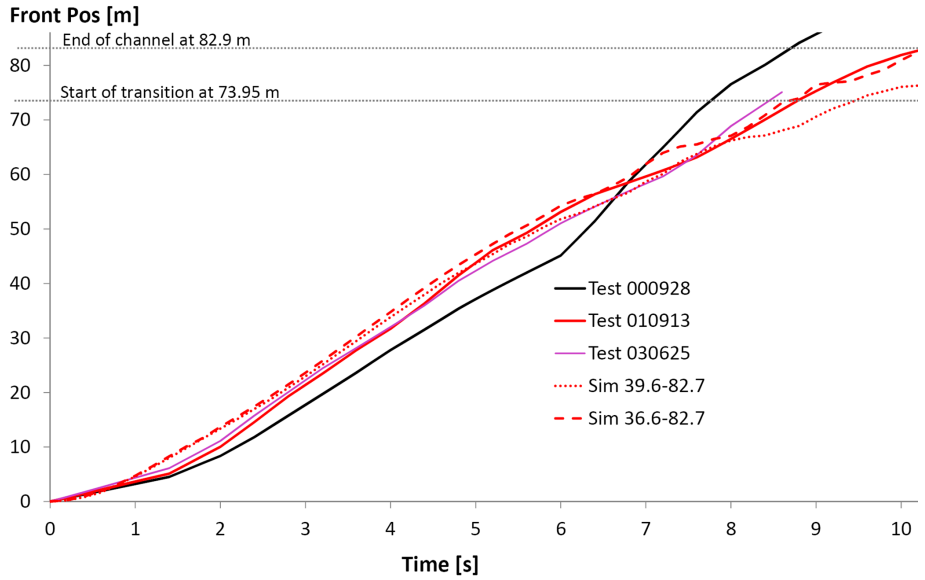

Figure 10. The flow front position over time of the rough-channel SGM mixture simulations, compared to three selected experiments of identical setup using the so-called SGM mixture, a standard mixture of sand, gravel and loam (Iverson et al., 2010). Based on the smooth channel calibration value $\tau_{00} = 90$ for 20.6 % water content, the corresponding value of $\tau_{00} = 82.8$ was applied for the SGM mixture with 17.9 % water content by applying Eq. (1). Since the bed roughness is overestimated by a representation as pyramids instead of half-spheres, one simulation used a reduced friction angle of 36.6° that corresponds to the lower boundary of possible experimental values based on published standard deviations (Iverson et al. (2010) (SGM and SG) in Table 3). The three tests experienced increasing front flow velocities after 5.5 s (black graph), 7 s (pink graph) or 7.4 s (red) as a second surge reached the flow front (observed from video, see Fig. 11).

GMDD
8, 6379–6415, 2015

Figure 11. Snapshots of the flow front of test 000928 (left) 5.6 s after release (bottom left) when the approaching second surge (top left) unified with the front. The same happened in test 010913 (center) 7.4 s after release (center bottom) and in test 030625 (right) 7.0 s after release (right bottom). The upper pictures were taken about half a second earlier in time than the lower row. The times of unification shown in the lower row coincided with a sudden increase in front velocity, see Fig. 10 .

GMDD
8, 6379–6415, 2015

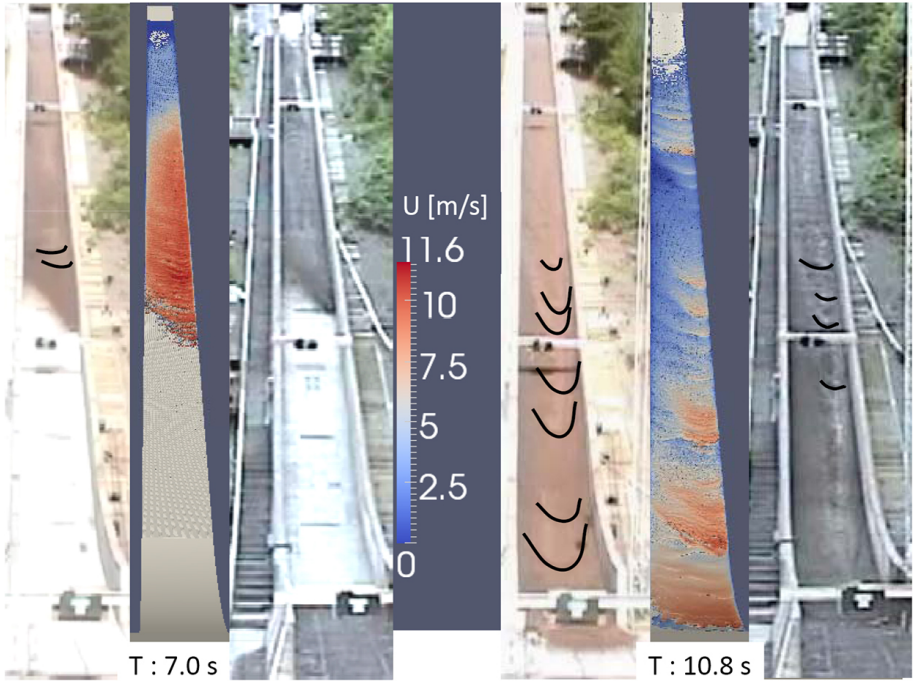

Figure 12. Comparison of the material surface in test 010913 (left of simulation) and test 030625 (right of simulation) at an intermediate position 7 s after release (left) and at the simulated front arrival at the run-out plane at 10.8 s (right) for a modeled friction angle of 36.6°. Black lines in the pictures highlight surface wave fronts, which appear more clearly in the video. In the simulation such waves are indicated by using the surface velocity as the color scale.

GMDD
8, 6379–6415, 2015

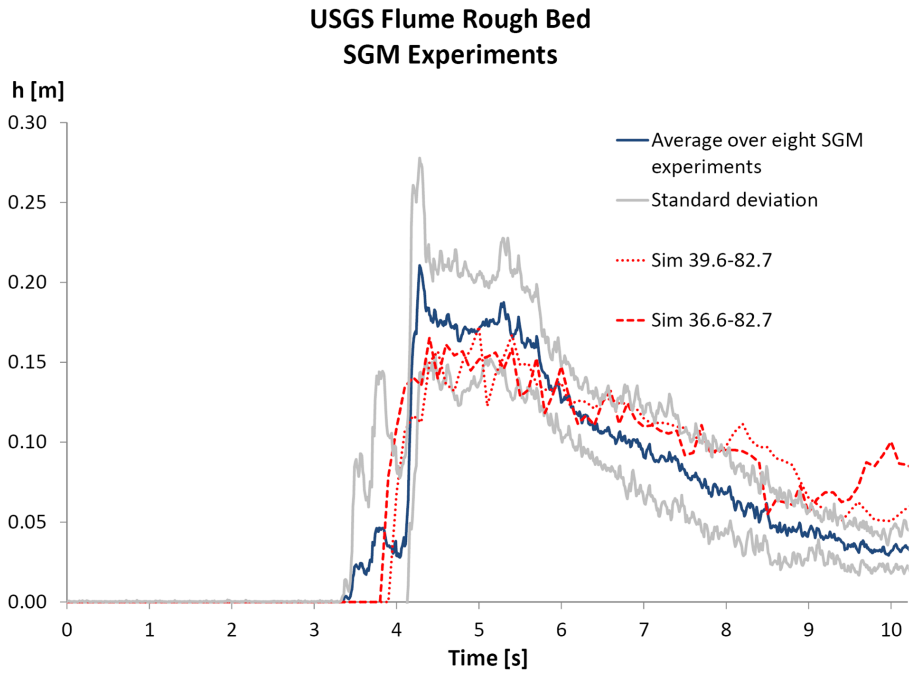

Figure 13. Comparison of simulated and measured flow heights 32 m downslope of the release gate. The measured values are derived as the average flow heads over all SGM mixture experiments, since no single-test data was accessible. In accord with the occurring second surge (see Fig. 11), the flow heads have another maximum about one second after the passing of the front peak.

GMDD
8, 6379–6415, 2015

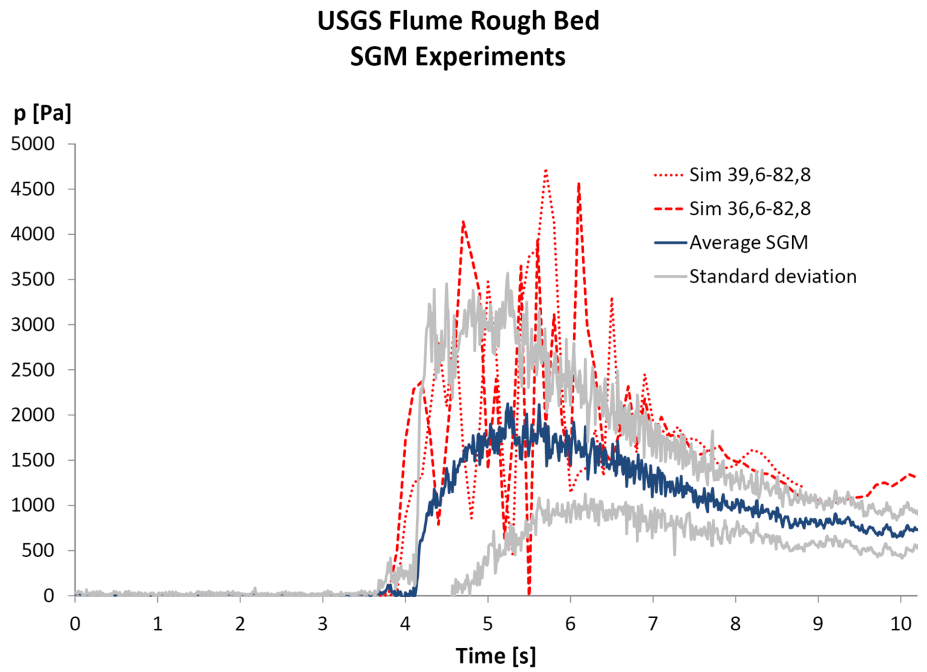

Figure 14. Comparison of simulated and measured basal normal stresses derived as the average temporal value of three force plates placed in the channel center line at 31.7, 32.3 and 32.9 m downslope from the release gate. The force plates were circular, however, three squares of basal cells with the same areas and positions as the force plates were used to derive the corresponding values in the simulation.

GMDD
8, 6379–6415, 2015